Proceedings of Ninth World Conference on Earthquake Engineering
August 2-9, 1988, Tokyo-Kyoto, JAPAN (Vol.III)

4-2-10

SEISMIC STABILITY OF NON-HOMOGENEOUS SOIL SLOPES

Chongpan JIN , Maotian LUAN and Gao LIN

Department of Civil Engineering, Dalian University of Technology, Dalian, China

SUMMARY

Based on the limit equilibrium principle and the variational technique, an efficient method for estimating the limit earthquake-resistant capacity of layered soil slopes is presented. Both non-homogeneity of soil properties and non-uniform distribution of seismic loads are considered. The concept of stability envelope is introduced for assessing the overall capacity of soil slopes subjected simultaneously to horizontal and vertical seismic loads. Abundant numerical results show the effects of factors associated with soil properties, slope geometry, and seismic loads on the yield seismic coefficient. Finally, a composite procedure for evaluating dynamic stability of non-homogeneous slopes is briefly proposed.

INTRODUCTION

Shortcomings of the conventional pseudo-static analyses on stability of slopes under seismic loading has been well known to all. Newmark (Ref. 1) first proposed the important concept that the seismic stability of slopes should be evaluated in terms of the potential displacements rather than the traditional minimum factor of safety, and developed a rigid-plastic sliding block model for predicting slope movements caused by seismic loading. Afterwards, several authors have made improvements to extend its practical application. The procedure includes two main steps, i.e., evaluation of critical limit states and prediction of displacements due to overloading.

Usually, the critical acceleration under which the slippage of the anticipated sliding mass can be initiated is called the yield acceleration a_y , which is often represented by the product of yield seismic coefficient k_y and the gravity acceleration g. Limit equilibrium principle and the upper bound theorem of limit analysis have been used to estimate the values of k_y for slopes with different failure mechanism such as plane and logarithmic spiral rupture surfaces (Refs. 2,3). The problem was studied experimentally too (Ref. 4).

It should be noted that only homogeneous soil slopes were investigated in the past. In fact, for practical slopes both the soil properties and the seismic loads are usually non-uniformly distributed with depth. These non-homogeneities may considerably affect the computational results. For this sake, they should be taken into account.

To solve the problem, the limit equilibrium principle is utilized

accompanied by the variational technique. Several relevant parameters are optimized through the extreme value condition of the functional constructed for the problem. This gives up elaborate computation efforts on the conventional trial and error process so that systemetic parameter studies are achieved.

FUNDAMENTALS OF THE METHOD

Basic Assumptions The slope consists of layered non-homogeneous but isotropic soil deposits, and each layer is designated with unit weight γ_i, cohesion c_i and friction angle ϕ_i. The effect of earthquake shaking is replaced by non-uniformly distributed pseudo-static loads. The magnitude of the load is represented by the product of seismic coefficient k and weight of the sliding mass, and the direction of application is supposed to make an angle of α_s with the horizontal. The slope is considered to have a sectional plane profile. A sketchy representation of profile characteristics and load distributions is shown in Fig.1.

For convenience, the following illustrations and computations will place emphasis upon typical two-layered slopes with α_0, α_1 and α_2 being zero, and no other forces but the soil weight and seismic loads are exerted on the slope.

Illustrations of Mathematical Formulation According to the limit equilibrium principle, three equations of equilibrium for the potential sliding mass are to be formulated. The relationship between normal stress σ and shear stress τ along the possible slip surface is considered to obey Coulomb's criterion

$$\tau(x) = c + \sigma(x) \tan\phi \tag{1}$$

For simplification, it is postulated that both soil cohesion c and seismic coefficient k are linear functions of depth. Therefore,

$$c = c_i = c_{i0} + m_{ci}\gamma_i(y - y_i), \quad \phi = \phi_i, \quad k = k_i = k_{i0}[1 - m_{ki}(y-y_i)/H]; \quad \text{for } y_{i-1} < y < y_i, \ i=1, 2 \tag{2}$$

where c_{i0}, m_{ci}, m_{ki} are designated parameters; k_{20} is a parameter to be determined by the optimization method, and its extreme value is called the datum value of the yield seismic coefficient under a given mode of acceleration distribution; H stands for the height of slope. All other symbols are shown in Fig.1.

For convenience of illustration and analysis, the following non-dimensional parameters and variables are introduced,

$$\bar{x} = x/H, \ \bar{y} = y/H, \ \bar{y}_i = y_i/H, \ \bar{D} = D/H, \ \bar{c}_{i0} = c_{i0}/\gamma H, \ \psi_i = \tan\phi_i, \ \beta_i = \gamma_i/\gamma \tag{3}$$

in which γ is the unit weight used for normalization, i=1,2. Along with all the expressions given above, it can readily be proven that the three equilibrium equations will take the form of

$$T_i = \int_{\bar{x}_A}^{\bar{x}_B} F_{i1}(\bar{x}, \bar{y}, \bar{y}', \bar{\sigma}) \, d\bar{x} + \int_{\bar{x}_B}^{\bar{x}_C} F_{i2}(\bar{x}, \bar{y}, \bar{y}', \bar{\sigma}) \, d\bar{x} = 0, \quad i=1, 2, 3, \tag{4}$$

where F_{ij}, i=1, 2, 3 and j=1, 2, are functions of $\bar{x}$, $\bar{y}$, $\bar{y}'$, $\bar{\sigma}$. They all vary with the parameters related to slope geometry, soil properties and load distribution. The explicit expressions will not herewith be labelled owing to limited space.

Without any difficulty, the preceding issue is to be reduced to a non-linear mathematical programming problem, namely,

$$\left.\begin{aligned} &\text{Min. } k_{20}(\bar{x}, \bar{y}, \bar{y}', \bar{\sigma}, \bar{x}_A, \bar{x}_B, \bar{x}_E, \bar{x}_D, \bar{x}_C) \\ &\text{S.t. } T_i = 0, \quad i=1, 2, 3 \end{aligned}\right\} \tag{5}$$

It is obvious that under a given value of m_{ki} and k_{10}/k_{20}, k_{20} is an implicit functional of $\bar{y}(\bar{x})$, $\bar{y}'(\bar{x})$ and $\bar{\sigma}(\bar{x})$. In order to overcome the mathematical difficulty manifested in directly solving this problem, the following composite functional is constructed by employing Lagrange's multiplier procedure and the variational technique,

$$\prod = \int_{\bar{x}_A}^{\bar{x}_B} S_1 \, dx + \int_{\bar{x}_B}^{\bar{x}_C} S_2 \, dx \tag{6}$$

where

$$S_j = F_{1j} + \lambda_1 F_{2j} + \lambda_2 F_{3j}, \qquad j=1, 2 \tag{7}$$

in which λ_1, λ_2 are Lagrange's multipliers to be determined. The use of the condition $\prod = 0$, combined with all related geometric boundary conditions, leads to the corresponding boundary-value issue. Euler's differential equations, integral conditions, transversity , refraction and geometric boundary conditions are outlined as following,

$$\partial S_i/\partial \bar{\sigma} = 0; \quad \partial S/\partial \bar{y} - d(\partial S_i/\partial \bar{y}')/d\bar{x} = 0, \quad i=1,2 \tag{8}$$

$$\text{Min } \prod = 0; \quad \partial \Pi/\partial \lambda_l = 0, \quad l=1,2 \tag{9}$$

$$\left.\begin{aligned} &[S_1 - (\bar{y}'-\bar{y}_o')\,\partial S_1/\partial \bar{y}']\Big|_{\bar{x}=\bar{x}_A} = 0; \quad (\partial S_{1+}/\partial \bar{y}' - \partial S_{1-}/\partial \bar{y}')\Big|_{\bar{x}=\bar{x}_E} = 0, \\ &\qquad\qquad \text{(only for the case of } \bar{x}_B > 0); \\ &\{[S_2 - (\bar{y}'-\bar{y}_1')\,\partial S_2/\partial \bar{y}'] - [S_1 - (\bar{y}'-\bar{y}_1')\,\partial S_1/\partial \bar{y}']\}\Big|_{\bar{x}=\bar{x}_B} = 0; \\ &(\partial S_{2+}/\partial \bar{y}' - \partial S_{2-}/\partial \bar{y}')\Big|_{\bar{x}=\bar{x}_D} = 0 \end{aligned}\right\} \tag{10}$$

$$\bar{y}_A = \bar{x}_A \tan\alpha_o, \quad \bar{y}_B = \bar{y}_1(\bar{x}_B), \quad \bar{y}_C = 1, \quad \bar{x}_C = 1/\tan\beta, \quad \bar{x}_E = 0, \quad \bar{x}_D = \bar{D}/\tan\beta \tag{11}$$

These equations can be solved by performing a coordinate transformation, i.e., $\bar{x} = \bar{r}\cos\theta + \bar{x}_r$, $\bar{y} = \bar{r}\sin\theta + \bar{y}_r$, where (r, θ) is the polar coordinate of the point (x,y) under consideration, $\bar{r} = r/H$; $\bar{x}_r = 1/\lambda_2$, $\bar{y}_r = \lambda_1/\lambda_2$. Consequently, the critical slip surface and its stress distribution mode can be obtained from equations (8). Furthermore, the solution of equations (9)-(11) yields nine nonlinear implicit equations concerning the unknown parameters θ_A, θ_B, θ_E, θ_D, θ_c, $\bar{r}_A$, k_{20}, $\bar{x}_r$ and $\bar{y}_r$,

$$W_j(\theta_A, \theta_B, \theta_E, \theta_D, \theta_c, \bar{r}_A, k_{20}, \bar{x}_r, \bar{y}_r) = 0, \qquad j=1, 2, \ldots, 9 \tag{12}$$

which simultaneously constitute the basic formulas to define the critical state of the slope. Details can be found in the authors' companion paper (Ref. 5).

Computational Approach A discrete Brown's algorithm, as an extended form of Newton's numerical approach, is employed to solve the nonlinear equation set (12). In this method, an iteration scheme is utilized which combines successive elimination of variables with a series of recursions, following a consecutive linearization procedure for each equation. A computer program adapted to microcomputers has been developed for performing enormous calculations.

RESULTS WITH DISCUSSIONS

Results 1. Failure mechanism. By solving Euler's equations (8), it can be directly proven that the most likely failure mechanism for layered $c-\phi-\gamma$ soil slope with non-homogeneity of cohesion is deep-seated sliding in concordance with a sectional logarithmic spiral surface. In addition, numerical results show that both the yield seismic coefficient and the actual shape of the rupture surface not only depend on the average soil strength and on the geometric characteristics, but also are intimately related to the variation of soil properties and seismic

loads with depth. As an example, Fig. 2 (a)~(d) portray the limit states of layered slopes with different ratio of D/H = 0, 0.4, 0.8, 1.0 respectively, where D denotes the upper layer thickness.

2. Effect of variation mode and direction of seismic load on k_y. Fig. 3 portrays the somewhat outstanding effect of variation mode of seismic load with depth on $\overline{k}_y$, where $\overline{k}_y$ denotes the average yield seismic coefficient weighted by the layer thickness. For practical computation, $\overline{k}_y$ should be weighted according to the sliding mass along depth.

In Fig. 4 shown is the stability envelope of soil slope subjected to horizontal and vertical seismic loads simultaneously. The horizontal and vertical components of yield seismic coefficient k_y constitute an outward convex envelope in the limit load space. It is seen that for practical slope angles the reduction of horizontal earthquake-resistant capacity due to upward vertical seismic load with k_v less than $2k_h/3$ may be up to 20%. And it must be pointed out that for definite combinations of β, ϕ and k_v/k_h, vertical seismic load may eccentrically effect the value of limit horizontal seismic coefficient k_{hy}.

3. Effect of soil cohesion and its variations on k_y. Fig. 5 indicates the increase of k_y with $\overline{c}$. It is worth noting that soil cohesion has considerable effect on the stability of slopes, but conventionally this effect is ignored. Furthermore, the effect of variation of soil cohesion with depth on k is also practically significant. It is observed from Fig. 6(a) that k_y is nearly directly proportional to m_c, where m_c denotes gradient of cohesion as defined in eq. (2). Fig. 6(b) shows that k_y is closely related to the ratio of cohesion of upper and lower layers. Fig. 7 gives a series of stability envelopes for a specific slope with different layeredly distributed cohesion.

4. Effect of layered variation of ϕ on k_y. It can be seen from Figs. 8, 9, 10(a),(b) that increase of average friction angle makes not only k_y increase for the case of $\alpha_s = 0$, but also the corresponding stability envelopes expand outwards. It is worth noting that layered distribution of ϕ has substantial influence on limit capacity of the slope. As an example, in Table 1 shown is the computational results for a slope composed of two layers with equal depth. Although the mean $\phi = \overline{D}\phi_1 + (1-\overline{D})\phi_2$ is identical for all cases, differences of k_y can fall in 50–75%.

Table 1 Effect of Variation of ϕ on k_y or k_{hy}

	k_y (k_{hy}) \ (β, α_s) / (ϕ_1, ϕ_2)	$\beta = 30^\circ$		$\beta = 45^\circ$	
		$\alpha_s = 0^\circ$	$\alpha_s = 20^\circ$	$\alpha_s = 0^\circ$	$\alpha_s = 30^\circ$
(1)	$\phi_1 = 30^\circ$, $\phi_2 = 20^\circ$	0.230	0.319(0.300)	0.190	0.197(0.171)
(2)	$\phi_1 = 20^\circ$, $\phi_2 = 30^\circ$	0.454	0.505(0.474)	0.315	0.344(0.298)
(3)	(2)/(1)	1.516	1.580	1.662	1.744

Discussions 1. It is not difficult to show that the solution of equation set (12) not only satisfies all equilibrium equations for the sliding mass, but also fulfills the condition that makes external work rate of a specific virtual velocity field equal to dissipation rate of the corresponding internal energy. Hence, this solution can be regarded as a certain minimum upper bound for the real solution.

2. By comparing the computational results with the test data from model sand slopes on a shaking table conducted in Tokyo University (Ref. 6) as shown in Fig. 11, in which $n_c = 1/\tan\beta$, the validity of the suggested solution is verified. The influence of cohesion on ultimate capacity of slope is revealed in Fig. 11.

3. The stability envelope diagram, as shown in Fig.4, is employed effectively to determine the state of the slope: stable state, or critical state, or over-loading state at a given instant during earthquake, according to the location the

seismic load point falls in the diagram: inside of, or just on, or outside of the envelope respectively. In the case of overloading, Newmark type analysis for evaluating the possible displacement during a specific earthquake (Ref. 5) can be applied. The authors have worked on a composite method which combines the determination of critical state of soil slope by the stability envelope with the assessment of movements under overloading. Details are to be provided in the continuation of this paper.

CONCLUSIONS

From the theoretical and numerical analyses, it has been concluded that non-homogeneities, either in soil properties or in distribution of seismic loads with depth have notable influence on yield acceleration and critical state of soil slopes. Emphasis should be placed upon the effect of soil cohesion and the vertical component of seismic loads on earthquake-resistant capacity of the slopes, and they are usually ignored in most studies.

The method for estimating yield seismic coefficient of soil slopes presented here can be successfully extended to more sophisticated cases such as embankment dams with clay core and anisotropic soil slopes.

REFERENCES

1. Newmark, N.M., "Effects of Earthquake on Dams and Embankments," Geotechnique, 15, 137-160, (1965).
2. Sarma, S.K., "Seismic Stability of Earth Dams and Embankments," Geotechnique, 25, 743-761, (1975).
3. Chang, C.J., Chen, W.F., and James, T.P.Yao, "Seismic Displacements in Slopes by Limit Analysis," J. of Geotechnical Engrg, ASCE, 110, 860-874, (1984).
4. Goodman, R.E., Seed, H.B., "Earthquake Induced Displacements in Sand Embankments," J. Soil Mech. & Fud. Div., ASCE, 92, 125-146, (1966).
5. Luan Maotian, Jin Chongpan, and Lin Gao, "Dynamic Stability of Nonhomogeneous Soil Slopes Under Non-uniformly distributed Seismic Loading," Journal of Hydraulic Engineering (in Chinese, to be published), (1988).
6. Ma Yuquan, "Study on the Stability of Embankments Under Earthquakes," (in Japanese), Research Reports of Technology Institute of Tokyo Univ., (1985).

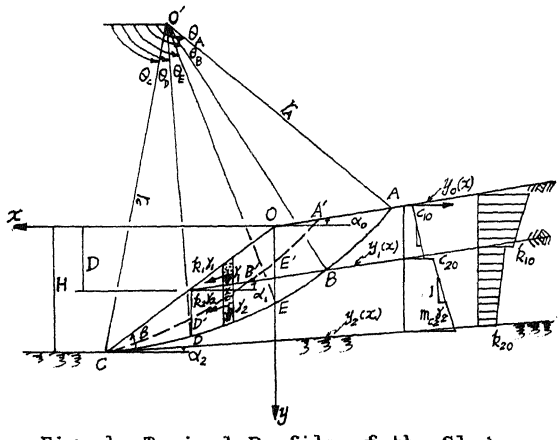

Fig. 1 Typical Profile of the Slopes

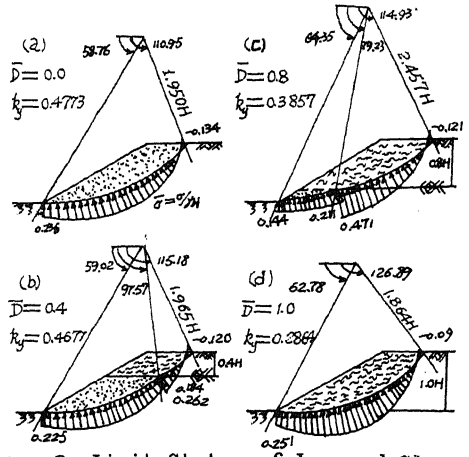

Fig. 2 Limit States of Layered Slopes (ϕ_1=20°, ϕ_2=30°, β=30°, $\bar{c}_1=\bar{c}_2=0.1$)

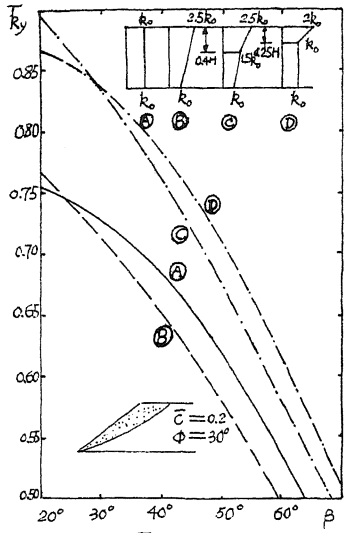

Fig. 3 $\bar{k}_y$ Under Various $m_{k_1}, m_{k_2}, k_{10}/k_{20}$

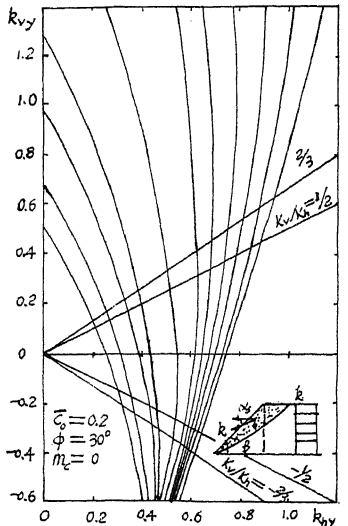

Fig. 4 Stability Envelopes of Slopes

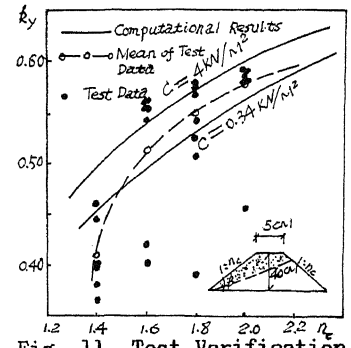

Fig. 11 Test Varification of Theoritical Results

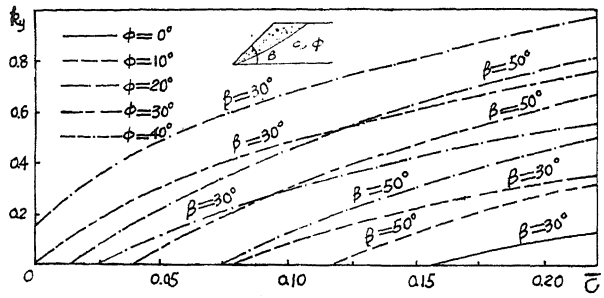

Fig. 5 Variations of k_y with $\bar{c}$

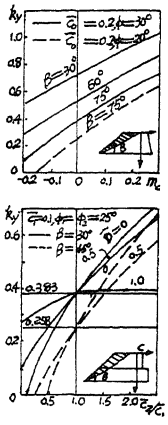

Fig. 6

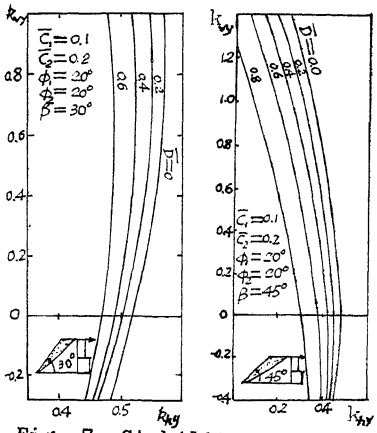

Fig. 7 Stability Envelopes of c-Layered Slopes

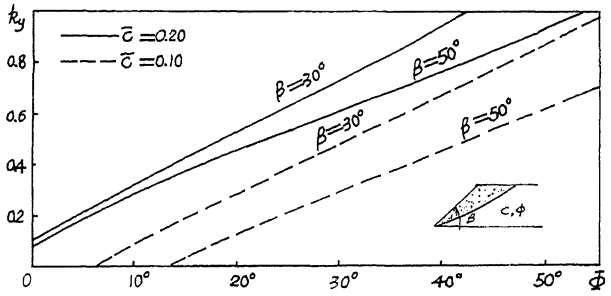

Fig. 8 Variations of k_y with

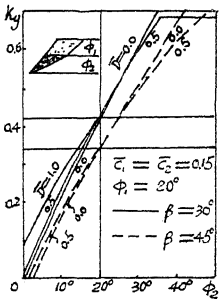

Fig. 9

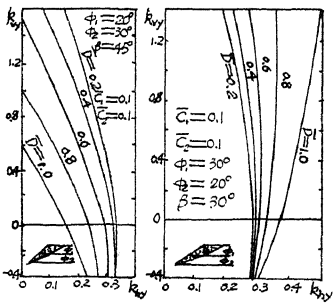

Fig. 10